



# Optimizing Power System Stability with Advanced Control Techniques in VSC-based HVDC Networks

Naser Taheri<sup>1\*</sup>, Mohammad Amin Salehi Mishani<sup>2</sup>, Mohammad Moein Yaghoubi<sup>3</sup>, Ehsan Akbari<sup>4</sup>

<sup>1</sup>Faculty Member, Department of Electrical Engineering, Technical and Vocational University (TVU), Tehran, Iran

<sup>2</sup>Department of Electrical Engineering, Azad University, Bushehr Branch, Bushehr, Iran

<sup>3</sup>Energy Management Department, New York Institute of Technology, Vancouver campus, Canada

<sup>4</sup>Department of Electrical Engineering, Mazandaran University of Science and Technology, Babol, Iran

---

## Abstract

The escalating demand for electrical power propels the evolution of power systems from regional to national scales. However, this expansion introduces challenges such as congestion and transmission bottlenecks, compromising system reliability and stability. High Voltage Direct Current (HVDC) systems, particularly those employing Voltage Source Converter (VSC) technology, offer promising solutions due to their unique control capabilities. This paper proposes the utilization of supplementary control alongside VSC-based HVDC to mitigate low-frequency oscillations and enhance dynamic and transient stability in power systems. Through a comprehensive investigation, including linearization of nonlinear power system equations, the efficacy of different input signals for supplementary control is evaluated using techniques like Singular Value Decomposition (SVD), Relative Gain Array (RGA), and Damping Function. The design of a phase compensator as a supplementary controller, employing generator speed deviation as input, is presented based on the linearized model. Additionally, recognizing the limitations of linear controllers in nonlinear systems, an adaptive neural network-based damping controller is proposed to improve dynamical and transient stability. Results demonstrate the effectiveness of the adaptive neural network controller over the phase compensator, particularly in stabilizing the power system and damping oscillations, underscoring the significance of considering nonlinear dynamics in controller design for HVDC systems.

Keywords: Power system dynamic stability, Adaptive Control, Supplementary Damping Controller, Neural Network Control, VSC HVDC

Article history: Received 2024/05/18; Revised 2024/07/10; Accepted 2024/07/25. Paper type: Research Paper

© 2024 IAUCTB-IJSEE Science. All rights reserved

<https://doi.org/10.82234/ijsee.2024.1120182>

---

## 1. Introduction

The ever-increasing demand for electrical power necessitates the continuous evolution of power systems, expanding from regional to national scales [1-3]. However, this expansion brings forth significant challenges such as congestion and transmission bottlenecks, which can compromise the reliability and stability of the entire system. In response to these challenges, High Voltage Direct Current (HVDC) systems, particularly those leveraging Voltage Source Converter (VSC) technology, emerge as promising solutions due to their unique control capabilities [4-7].

VSC HVDC systems have revolutionized power transmission by offering enhanced dynamic stability compared to traditional HVAC systems. By decoupling the transmission of active and reactive power, VSC HVDC systems enable independent control of power flow and voltage, thus improving

system stability under varying operating conditions [8-11]. Inside a VSC HVDC system, various control loops are employed to regulate different aspects of the converter operation. These include voltage control loops to maintain the desired DC voltage level, current control loops to regulate the output current waveform, and power control loops to manage active and reactive power exchange with the AC grid [12-14]. In addition to these primary control loops, supplementary damping controllers are often integrated into VSC HVDC systems to mitigate power oscillations and enhance stability. These controllers, such as power oscillation damping (POD) controllers, utilize signals from the AC grid to generate supplementary control signals that are injected into the converter control system [15-20].

Optimal input-output signal coupling is essential for the design of effective damping

controllers in VSC HVDC systems. By ensuring proper coupling between input and output signals, the controller can effectively dampen power oscillations and improve system stability. Techniques such as Relative Gain Array (RGA) criteria and Singular Value Decomposition (SVD) are utilized to identify the most significant input-output couplings, guiding the design of robust damping controllers [1-3].

In addition to conventional damping controllers, adaptive neural network-based controllers offer a promising alternative for enhancing the dynamic stability of VSC HVDC systems. These controllers leverage artificial intelligence techniques to adaptively learn and optimize control actions based on real-time system dynamics. By continuously adjusting their parameters, adaptive neural controllers can effectively mitigate power oscillations and improve transient stability, even in the presence of nonlinearities and uncertainties in the system.

This paper presents a dynamic model of a power system equipped with VSC HVDC, which can be utilized for dynamic studies and simulations in power system analysis. Furthermore, this study introduces novel criteria based on Singular Value Decomposition (SVD) and Relative Gain Array (RGA) for optimal coupling between input and output signals in VSC HVDC systems. These criteria provide valuable insights into the selection of input signals for supplementary control, enhancing the effectiveness of damping controllers. Additionally, a novel adaptive neural controller design is proposed, strategically placed in the appropriate path between input and output signals, to dampen oscillations in the power system. Through innovative approaches like these, the study aims to advance the state-of-the-art in control strategies for VSC HVDC systems, ultimately improving the stability and reliability of power grids. Simulation results show the effectiveness of the proposed control strategy for damping power and frequency oscillations.

## 2. Modelling of a Power System Equipped by VSC HVDC

Three distinct modeling approaches for Voltage Source Converter (VSC) High Voltage Direct Current (HVDC) systems are recognized in literature. The electromagnetic model, primarily employed for detailed equipment investigations, captures electromagnetic transients within the millisecond range, representing VSCs using switches [11]. While suitable for detailed equipment analysis, this model lacks applicability in power oscillation studies. The steady-state model, on the other hand, is tailored for assessing the steady-state

performance of power systems and computing initial operating conditions for dynamic studies [12]. Meanwhile, the dynamic model integrates dynamic equations of the power system with VSC HVDC dynamic equations, facilitating power system stability and transient studies [20,21].

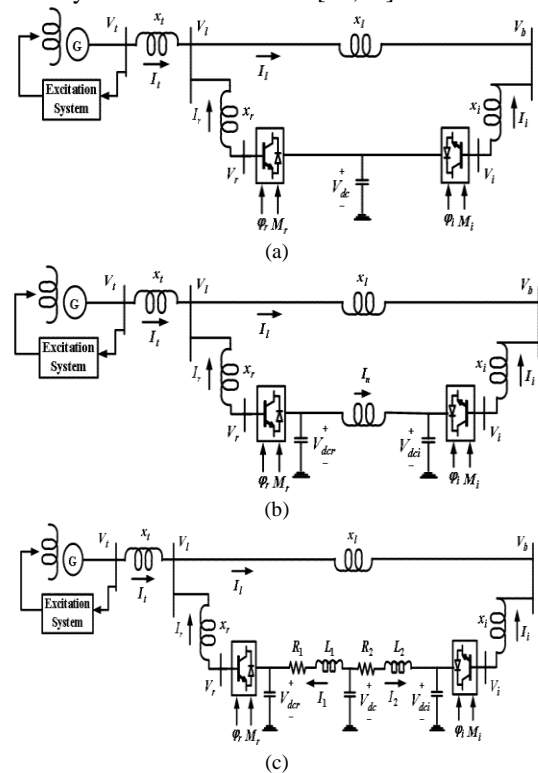


Fig.1 SMIB system equipped with a VSC HVDC (a)BtB VSC HVDC (b) VSC HVDC (c)Whole VSC HVDC

Figure 1 illustrates three configurations of Single Machine Infinite Bus (SMIB) systems integrated with VSC HVDC. The first model depicts a Back-to-Back VSC HVDC setup [11], while the second showcases a VSC HVDC system with a DC line [12-13]. Previous studies [19-20] have highlighted the potential of HVDC systems in enhancing power system stability through supplementary controller implementation and have investigated the controllability of system inputs using singular value decomposition. However, it's noteworthy that the resistance of DC cables utilized in HVDC transmission systems has not been explicitly modeled. The third configuration depicts the entire system of VSC HVDC, which serves as the focus of this study.

The Infinite Bus configuration is supplied by a High Voltage Alternating Current (HVAC) system parallel connected with a Voltage Source Converter (VSC) HVDC power transmission system. Each converter's AC side is linked to the line via a coupling transformer. The first voltage source converter functions as a rectifier, regulating the DC link voltage and maintaining voltage magnitude at

the connected terminal. Meanwhile, the second voltage source converter serves as a controlled voltage source, managing power flow in the VSC HVDC feeder. The four input control signals to the VSC HVDC are represented by  $M_r, \phi_r, M_i, \phi_i$ , where  $M$  and  $\phi$  denote the amplitude modulation ratio and phase angle of the control signals of each VSC, respectively. Utilizing Park's transformation and neglecting the resistance and transients of the coupling transformers, the VSC HVDC system (depicted in Fig. 1c) can be effectively modeled. Similarly, Figures 1a and 1b can be modeled utilizing the same approach.

$$\begin{bmatrix} V_{id} \\ V_{iq} \end{bmatrix} = \begin{bmatrix} 0 & x_r \\ -x_r & 0 \end{bmatrix} \begin{bmatrix} I_{rd} \\ I_{rq} \end{bmatrix} + \begin{bmatrix} (M_r V_{dcr} \cos(\phi_r))/2 \\ (M_r V_{dcr} \sin(\phi_r))/2 \end{bmatrix} \quad (1)$$

$$\begin{bmatrix} V_{bd} \\ V_{bq} \end{bmatrix} = \begin{bmatrix} 0 & x_i \\ -x_i & 0 \end{bmatrix} \begin{bmatrix} I_{id} \\ I_{iq} \end{bmatrix} + \begin{bmatrix} (M_i V_{dci} \cos(\phi_i))/2 \\ (M_i V_{dci} \sin(\phi_i))/2 \end{bmatrix} \quad (2)$$

$$CV_{dc} = -(I_1 + I_2) \quad (3)$$

$$L_1(dI_1/dt) = V_{dc} - V_{dcr} - R_1 I_1 \quad (4)$$

$$L_2(dI_2/dt) = V_{dc} - V_{dci} - R_2 I_2 \quad (5)$$

Where  $V_1, V_b$  represent the middle bus voltage and infinite bus voltage, respectively. the  $I_r, I_i$  denote current flowing into the rectifier and inverter, respectively.  $C$  and  $V_{dc}$  represent the DC link capacitance and voltage, respectively. Additionally,  $C_r, V_{dcr}$  represent the DC capacitance and voltage of the rectifier, while  $V_{dci}, C_i$  denote the DC capacitance and voltage of the inverter, respectively.

The non-linear model of the Single Machine Infinite Bus (SMIB) system depicted in Figure 1 is:

$$\dot{\delta} = \omega_b(\omega - 1) \quad (6)$$

$$\dot{\omega} = (P_m - P_e - D\omega)/M \quad (7)$$

$$\dot{E}'_q = (E_{fd} - (x_d - x'_d)I_t - E'_q)/T'_{do} \quad (8)$$

$$\dot{E}_{fd} = (K_A(V_{ref} - V_t + u_{pss}) - E_{fd})/T_A \quad (9)$$

Where:  $P_e = V_{id}I_{id} + V_{iq}I_{iq}$ ,  $V_t = \sqrt{V_{id}^2 + V_{iq}^2}$ ,

$V_{id} = x_q I_{iq}$ ,  $V_{iq} = E'_q - x'_d I_{id}$ ,  $I_{id} = I_{ld} - I_{rd}$ ,

are the input and  $P_e$  and  $P_m$  where  $I_{iq} = I_{iq} - I_{rq}$  output power, respectively;  $M$  and  $D$  the inertia constant and damping coefficient, respectively;  $\omega_b$  the synchronous speed; the rotor angle  $\omega$  and  $\delta$  and speed, respectively;  $E'_q, E'_{fd}$  and  $V_t$  the generator internal, field and terminal voltages, respectively;  $T'_{do}$  the open circuit field time constant;  $x_d, x'_d$  and  $x_q$  the d-axis, d-axis transient reactance, and q-axis reactance, respectively; the  $T_A$  and  $K_A$

exciter gain and time constant, respectively;  $V_{ref}$

the reference voltage. Also, from Fig. 1.c we have:

$$\bar{V}_t = jx_t \bar{I}_t + \bar{V}_l \quad (10)$$

$$\bar{V}_t = jx_t \bar{I}_t + jx_l \bar{I}_l + \bar{V}_b \quad (11)$$

$$\bar{I}_l = \bar{I}_t - ((\bar{V}_t - jx_t \bar{I}_t - \bar{V}_r)/jx_r) \quad (12)$$

Where  $\bar{I}_t, \bar{V}_r$  are the armature current,  $\bar{V}_b$  and  $\bar{I}_l$  rectifier voltage, infinite bus current and voltage respectively. From Eq (10)-(12) we can have:

$$I_{tq} = ((1/2x_r)(x_l M_r V_{dcr} \cos(\phi_r)) + V_b \sin(\delta))/(Zx_q + A) \quad (13)$$

$$I_{td} = (ZE'_q - (1/2x_r)x_l M_r V_{dcr} \sin(\phi_r) - V_b \cos(\delta))/(Zx'_d + A) \quad (14)$$

And For inverter side:

$$I_{id} = (-V_b \cos(\delta) + 0.5M_i V_{dci} \sin(\phi_i))/x_i \quad (15)$$

$$I_{iq} = (V_b \sin(\delta) - 0.5M_i V_{dci} \cos(\phi_i))/x_i \quad (16)$$

By linearizing Eq (1)-(7), (13)-(16):

$$\Delta\delta = \omega_b \Delta\omega \quad (17)$$

$$\Delta\dot{\omega} = (\Delta P_m - \Delta P_e - D\Delta\omega)/M \quad (18)$$

$$\Delta\dot{E}'_q = (\Delta E_{fd} - (x_d - x'_d)\Delta I_t - \Delta E'_q)/T'_{do} \quad (19)$$

$$\Delta\dot{E}_{fd} = (K_A(\Delta V_t + \Delta u_{pss}) - \Delta E_{fd})/T_A \quad (20)$$

Where:

$$\Delta V_t = K_5 \Delta\delta + K_6 \Delta E'_q + K_{vdcr} \Delta V_{dcr} \quad (21)$$

$$+ K_{vMr} \Delta M_r + K_{v\phi r} \Delta \phi_r \quad (22)$$

$$\Delta P_e = K_1 \Delta\delta + K_2 \Delta E'_q + K_{pdcr} \Delta V_{dc} \quad (23)$$

$$+ K_{pMr} \Delta M_r + K_{p\phi r} \Delta \phi_r \quad (24)$$

$$\Delta E'_q = K_4 \Delta\delta + K_3 \Delta E'_q + K_{qdcr} \Delta V_{dcr} \quad (25)$$

$$+ K_{qMr} \Delta M_r + K_{q\phi r} \Delta \phi_r \quad (26)$$

$$\Delta V_{dcr} = C_{31} C_r \Delta\delta + C_{32} C_r \Delta E'_q \quad (27)$$

$$+ C_{33} C_r \Delta V_{dcr} + C_r \Delta I_1 \quad (28)$$

$$+ C_{34} C_r \Delta M_r + C_{35} C_r \Delta \phi_r \quad (29)$$

Substitute Eq(21)-(23) in (17)-(20) we can obtain the state variable of the power system installed with the VSC HVDC to be(state space model):

$$\dot{X} = AX + BU \quad (30)$$

and

$X$

$$= [\Delta\delta, \Delta\omega, \Delta E'_q, \Delta E_{fd}, \Delta V_{dcr}, \Delta I_1, \Delta V_{dc}, \Delta I_2, \Delta$$

$$U = [\Delta M_r, \Delta \phi_r, \Delta M_i, \Delta \phi_i, u_{pss}]$$

Where:

$\Delta M_i, \Delta M_r, \Delta \phi_i, \Delta \phi_r$  and  $u_{pss}$  are the linearization of the input control signals of the VSC HVDC and PSS output i.e. modulation index of inverter, modulation index of rectifier, modulation angle of inverter, modulation angle of rectifier and input signal of PSS, respectively.

The linearized dynamic model of Eq.25 can be shown by Fig.2. In this figure  $K_{pu}, K_{qu}, K_{vu}, K_r$

and  $K_i$  are defined below:

$$K_{vu} = [K_{vMr}, K_{v\phi r}, 0, 0, 0],$$

$$K_{pu} = [K_{pMr}, K_{p\phi r}, 0, 0, 0],$$



### 3. Proposed Damping Controller Design

Damping controllers are devised to generate an electrical torque synchronized with the speed deviation. The modulation of the four control parameters of the HVDC enables the production of the damping torque, with the speed deviation serving as the input to the damping controllers.

#### A) Classic Compensator Design

The architecture of the HVDC-based damping controller is depicted in Figure 4, comprising gain, signal washout, and phase compensator blocks. The signal washout, acting as a high-pass filter, prevents steady speed changes from affecting the VSC HVDC input parameter. The washout time constant  $T_w$  should be sufficiently high to preserve signals associated with rotor speed oscillations. The specific value of  $T_w$  is not critical and may range from 1s to 20s. For our study,  $T_w$  is set to 10s. The parameters of the damping controller are determined using the phase compensation technique [25]. The following step-by-step procedure outlines the computation of damping controller parameters using the phase compensation technique:

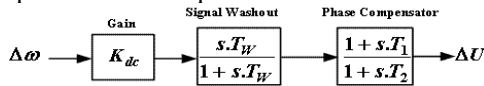


Fig.4 Structure of lead-lag controller

1. Computation of natural frequency of oscillation  $\omega_n$  from the mechanical loop.

$$\omega_n = \sqrt{K_1 \omega_0 / M} \quad (26)$$

2. Computation of  $\angle GEPA$  at  $s = j\omega_n$ . Let it be  $\gamma$ .

3. Design of phase lead/lag compensator  $G_C$ :

The phase lead/lag compensator  $G_C$  is designed to provide the required degree of phase compensation. For 100% phase compensation,

$$\angle G_C(j\omega_n) + \angle GEPA(j\omega_n) = 0 \quad (27)$$

Assuming one lead-lag network, the  $T_1 = aT_2$  transfer function of the phase compensator becomes,

$$G_C(s) = (1 + saT_2)/(1 + sT_2) \quad (28)$$

Since the phase angle compensated by the lead-lag network is equal to  $-\gamma$ , the parameters  $a$  and  $T_2$  are computed as,

$$a = (1 + \sin(\gamma))/(1 - \sin(\gamma)) \quad (29)$$

$$T_2 = 1/(\omega_n \sqrt{a})$$

4. Computation of optimum gain  $K_{dc}$  for desired damping.

#### B) Adaptive Damping VSC HVDC based Controller Design Using Neural Network

This section serves to provide a foundational understanding of neural networks (NN), with a particular focus on concepts relevant to their application in closed-loop control of discrete-time

dynamical systems. It delves into various aspects of NNs, including their diverse topologies, memory recall properties, fundamental characteristics, training methodologies, and architectural configurations. By exploring these key topics, readers will gain insights into the theoretical underpinnings and practical considerations essential for comprehending NN-based control systems.

In the work referenced as [24], researchers propose an adaptive neural controller tailored for integration into the Voltage Source Converter High Voltage Direct Current (VSC HVDC) model, as depicted in Figure 5. This adaptive neural controller comprises two distinct neural networks: an identifier and a controller. The identifier network serves to discern the system dynamics and characteristics, effectively capturing the underlying behavior of the VSC HVDC system. Meanwhile, the controller network leverages this acquired knowledge to dynamically adjust control signals, thereby optimizing system performance and stability. By delineating these components, the study offers a comprehensive framework for employing neural network-based controllers in enhancing the operation and efficiency of VSC HVDC systems.

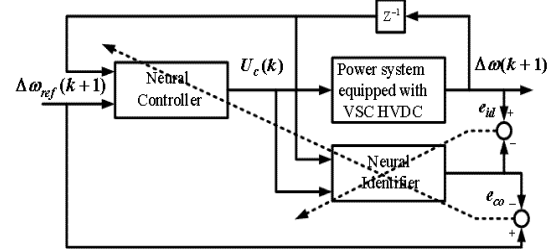


Fig.5 Structure of the online neural controller

The neural identifier, as depicted in Figure 6, serves as a crucial component within the adaptive neural controller. Its architecture consists of layers of interconnected neurons, where each neuron applies an activation function to its input signals to produce an output. In this context, the activation function employed is the hyperbolic tangent, denoted as  $f$ .

Training the neural identifier involves the error backpropagation method, a fundamental technique in neural network learning. This process begins with defining a cost function  $E_{id}$ , which quantifies the disparity between the actual rotor speed deviation  $\Delta\omega$  and the predicted deviation  $\widehat{\Delta\omega}$  generated by the neural identifier. The cost function is formulated as:

$$E_{id} = 0.5(\Delta\omega - \widehat{\Delta\omega})^2 = 0.5e_{id}^2 \quad (30)$$

where  $E_{id}$  represents the error between the predicted and actual values. To adjust the neural identifier's parameters (weights), the gradient of the cost function with respect to these parameters is computed using the chain rule of calculus. Specifically, the derivative of  $E_{id}$  with respect to the

output neuron's input  $V$  and weights  $\widehat{\Delta\omega}$  is determined as follows:

$$\frac{\partial E_{id}}{\partial(\widehat{\Delta\omega})} = -(\Delta\omega - \widehat{\Delta\omega}) = -e_{id} \quad (31)$$

$$\frac{\partial E_{id}}{\partial w_{oh}^{id}} = \left(\frac{\partial E_{id}}{\partial e_{id}}\right) \left(\frac{\partial e_{id}}{\partial(\widehat{\Delta\omega})} \times \frac{\partial(\widehat{\Delta\omega})}{\partial v}\right) \left(\frac{\partial v}{\partial w_{oh}^{id}}\right) \quad (32)$$

where  $v$  represents the weighted sum of inputs to the output neuron. Utilizing this gradient information, the weights between the output and hidden layers  $w_{oh}^{id}$  are updated iteratively to minimize the cost function:

$$w_{ohnew}^{id} = w_{ohold}^{id} - \eta \frac{\partial E_{id}}{\partial w_{oh}^{id}} \quad (33)$$

where  $\eta$  represents the learning rate, controlling the size of weight updates during each iteration. Through this iterative process, the neural identifier learns to approximate the relationship between the input signals and the rotor speed deviation, facilitating accurate prediction and control within the adaptive neural controller framework.

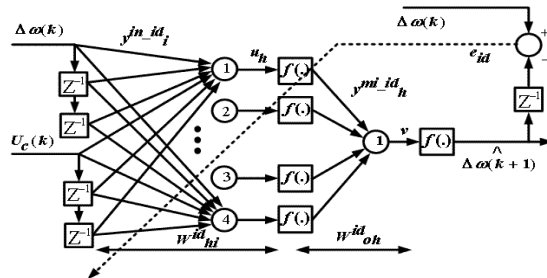


Fig.6 Structure of the online neural identifier

Structure of neural identifier is shown in Fig.7. This is a feed forward network. Back propagation method used to train this network as described in following. Coast function to training this network is:

$$E_{co} = 0.5(0 - \widehat{\Delta\omega})^2 = 0.5\widehat{\Delta\omega}^2 = 0.5e_{co}^2 \quad (34)$$

and

$$\frac{\partial E_{co}}{\partial(\widehat{\Delta\omega})} = \widehat{\Delta\omega} = -e_{co} \quad (35)$$

$$\frac{\partial E_{co}}{\partial w_{oh}^{co}} = \left(\frac{\partial E_{co}}{\partial e_{co}}\right) \left(\frac{\partial e_{co}}{\partial(\widehat{\Delta\omega})}\right) \times \frac{\partial(\widehat{\Delta\omega})}{\partial v} \left(\frac{\partial v}{\partial w_{oh}^{co}}\right) \quad (36)$$

$V$ ,  $w_{oh}^{co}$  are the neural identifier output and the weights between output and hidden layer of neural controller, respectively.

$$v = \sum_h \omega_{oh}^{id} y_h^{mi\_id} \quad (37)$$

$$y_h^{mi\_id} = f\left(\sum_i \omega_{hi}^{id} y_i^{in\_id}\right) = f(u_h)$$

$y_i^{in\_id}$ ,  $y_h^{mi\_id}$ ,  $\omega_{hi}^{id}$ ,  $\omega_{oh}^{id}$ ,  $i$  and  $h$  are inputs, inputs to output layer, connection weights between input and hidden layer, weights between output and hidden layer, number of inputs and number of

neuron in hidden layer of neural identifier, respectively. So:

$$\left(\frac{\partial v}{\partial w_{oh}^{co}}\right) = \left(\frac{\partial v}{\partial U_c}\right) \left(\frac{\partial U_c}{\partial w_{oh}^{co}}\right) = \quad (38)$$

$$(\partial v / y_h^{mi\_id}) (y_h^{mi\_id} / \partial U_c) (\partial U_c / \partial w_{oh}^{co})$$

Using equations (36-38), it is possible to calculate the sensitive coefficient in output neuron of neural controller and correct the middle and output weights of neural controller.

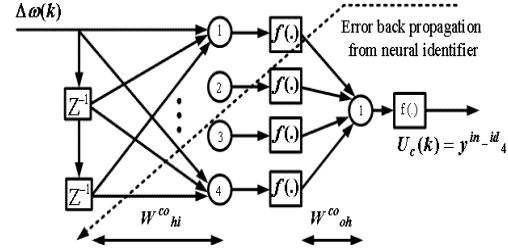


Fig.7 Structure of the online neural controller

### C) Control Structure Survey based on SVD, RGA, Damping Function Concepts

To damp power system oscillations using VSC HVDC, control structure design is clearly important due to the complexity of power systems. Control structure design includes selecting inputs and outputs for a supplementary damping controller, which has the most effectiveness on system behavior. It governs how the supplementary damping controller interacts with the power system to mitigate oscillations and enhance stability.

From a physical understanding of the power system, it is clear that the best choice for an output in stability issues is the deviation of rotor speed. However, according to Equation 25, it is evident that a power system equipped with a VSC HVDC line is a multivariable system, making input selection crucial for designing a controller. Equation 25 highlights the multivariable nature of the power system, indicating the need for careful consideration in selecting inputs for optimal controller design.

So in this section, SVD and RGA are used for input selection. Singular Value Decomposition (SVD) and Relative Gain Array (RGA) are mathematical techniques employed to analyze the input-output relationships and interactions within the multivariable power system, aiding in the selection of inputs for the supplementary damping controller.

The smallest singular value of the plant, denoted as  $\underline{\sigma}(G)$ , assessed across frequency, serves as a valuable metric for determining the feasibility of achieving satisfactory control outcomes. When inputs and outputs undergo scaling, it becomes feasible to generate an output magnitude of at least  $\underline{\sigma}(G)$  in any output direction with a manipulated input of unit magnitude, as measured by the 2-norm.

Generally, to prevent input saturation, it is preferred that  $\sigma(G)$  exceed 1 across all frequencies necessitating control. Interested readers are directed to [26] for more comprehensive insights.

In the subsequent discussion, the application of Singular Value Decomposition (SVD) is elucidated for the selection of the system's output. Assessing the controllability of the Electromechanical (EM) mode by a designated input (control signal) involves employing SVD [22-23-24]. Mathematically, if  $G$  represents an  $m \times n$  complex matrix, then there exist unitary matrices  $U$  and  $V$  with dimensions of  $m \times m$  and  $n \times n$ , respectively, satisfying:  $G = U\Sigma V^H$  Here,  $\Sigma$  denotes an  $n \times m$  matrix containing nonnegative real numbers along the diagonal. The minimum singular value  $\sigma_{min}$  serves to quantify the distance of matrix  $G$  from all matrices having a rank equivalent to  $\min(m, n)$ , offering a means to gauge modal controllability.

The minimum singular value,  $\sigma_{min}$  of matrix  $G$ , indicates the capability of the  $n$  input to regulate the mode associated with eigenvalue  $\lambda$ . Consequently, higher  $\sigma_{min}$  values correspond to increased mode controllability by the selected input. As such, evaluating the controllability of the EM mode with all inputs facilitates identification of the most effective input for oscillation mode control.

"A straightforward yet potent screening tool for input and output selection, circumventing combinatorial challenges, is the Relative Gain Array (RGA). Its inception can be traced to [27], furnishing designers with a swift means to gauge interaction within multivariable system control loops. For an  $l \times m$  matrix  $G$ , RGA is delineated as:

$$RGA(G) = \Lambda(G) = G \times (G^l)^T \quad (39)$$

Here,  $G^l$  symbolizes the pseudo-inverse,  $(.)^T$  denotes transposition, and  $\times$  signifies element-wise multiplication. RGA harbors several salient control properties. In cases with numerous input manipulations, columns with sums markedly below 1 may warrant exclusion. Similarly, in scenarios with manifold output candidates, rows with sums significantly under 1 may merit omission [26].

Thus, RGA unveils the interplay among diverse input/output pairs on the overall system. This aspect is pivotal in gauging input controllability: the sum of the  $i$ -th row in RGA corresponds to the square of the  $i$ -th output projection, while the sum of the  $j$ -th column equates to the square of the  $j$ -th input projection. Further elucidation can be found in [26, 27].

In [28], RGA was employed to assess input controllability in a Back-to-Back (BtB) VSC HVDC system. The method involved solving Equation 25 for each low frequency, followed by computation

and graphical representation of  $G(j\omega)$  and the row-wise summation. This approach facilitated the identification of the primary input for applying the damping signal derived from the supplementary controller.

The linearized model of the power system installed with the BtB VDC HVDC can be expressed by Fig. 8 [29], where  $H(s)$  is the transfer function of the HVDC damping controller. From Fig. 8 we can obtain the electric torque provided by the HVDC damping controller to the electromechanical oscillation loop of the generator to be:

$$\begin{aligned} \Delta T_{HVDC} &= (K_c(\lambda_0)K_0(\lambda_0)H(\lambda_0) \\ &/(1 - K_{IL}(\lambda_0)H(\lambda_0)))\Delta\omega \end{aligned} \quad (40)$$

An ideal HVDC damping controller should contribute a pure positive damping torque to the electromechanical oscillation loop with  $\Delta T_{HVDC} = D_{HVDC}\Delta\omega$  that is:

$$D_{HVDC} = (K_c(\lambda_0)K_0(\lambda_0)H(\lambda_0) / (1 - K_{IL}(\lambda_0)H(\lambda_0))) \quad (41)$$

which results in:

$$D_{HVDC} = [K_c(\lambda_0)K_0(\lambda_0) + D_{HVDC}K_{IL}(\lambda_0)H(\lambda_0) = F(\lambda_0)H(\lambda_0)] \quad (42)$$

$F(\lambda_0)$  which is named as the forward path of the BtB VSC HVDC damping controller, has a decisive influence on the effectiveness of the HVDC damping controller.

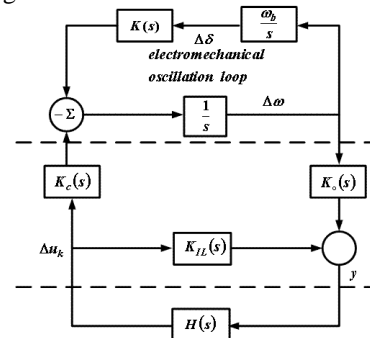


Fig.8. Closed-loop system installed with UPFC dumping controller

If we assume the set of the operating conditions of the power system is  $\Omega(\mu)$ ,  $F(\lambda_0)$  can be denoted as the function of system operating condition  $\mu$  and input control signal of the HVDC  $u_k$ . The criterion of the selection can be [29]:

$$\mu_{selected} = \min F(\lambda_0, \mu, u_k), \mu \in \Omega(\mu) \quad (43)$$

$$u_{selected} = \max_{u_k} F(\lambda_0, \mu_{selected}, u_k) \quad (44)$$

$$u_k \in \{M_r, M_i, \phi_r, \phi_i\} \quad (45)$$

$$u_{selected} = \max F(\lambda_0, \mu_{selected}, u_k), u_k \in \{M_r, M_i, \phi$$

a) Eq.43 requires that the operating condition, where the HVDC damping control is least

effective, is selected for the design of the controller.

- b) For the efficient operation of the HVDC damping function. The required damping should be provided at minimum control cost.
- c) A good design of damping controller requires that it provides a steady damping over all the range of power system operating conditions.

Furthermore, from Eq.42 we can see that the phase compensation method can be used to set the parameters of the HVDC damping controller.

#### 4. Simulation Results

To evaluate the capabilities of the proposed control, MATLAB software is used to simulate the power system along with the additional controllers. All system data is provided in the appendix of the article. Mechanical power changes in the turbine are used as disturbances in the linearized system. In the non-linear system, a three-phase short circuit is used to assess the performance of the proposed controllers.

To design the supplementary stabilizer controller described in this article, it is essential to determine the appropriate coupling between input and output signals based on the provided dynamic model. This ensures the optimal and robust performance of the supplementary controller. Accordingly, the RGA criteria (used to measure the interference of an input-output coupling with other couplings) and SVD criteria (used to identify the input with the greatest effect on the electromechanical mode of the power system) are employed. The damping function also provides the optimal operating point for additional controller design.

To select the coupling of input and output signals with minimal interference with other control channels, the sum of the columns of the RGA matrix is calculated for frequencies below 20 Hz. Based on this calculation, the input with the highest sum of RGA values across different frequencies has less interference with the other existing control channels.

The results of these calculations are shown in Figure 9. It can be seen that the input related to the modulation angle of the rectifier in VSC HVDC has less interference compared to other inputs. Additionally, the input related to the power system stabilizer (PSS) also shows less interference than other system inputs. However, in the case of inverter control inputs, the signal coupling interference is significant.

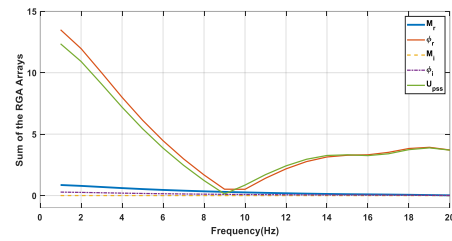


Fig.9. RGA Results

The SVD criterion was introduced to select the input with the most significant effect on strengthening the oscillation mode damping of the power system. In this article, the SVD values of the controllability matrix are calculated for different operating points of the system as well as certain inputs, and the smallest singular value of this matrix is plotted. The input with the smallest singular value, compared to the values corresponding to other inputs, has the greatest effect on the oscillation mode. The results of applying the SVD criterion are shown in Figure 10. It can be seen that the phase angle of the rectifier and the phase angle of the inverter have the greatest effect on the oscillatory modes of the power grid.

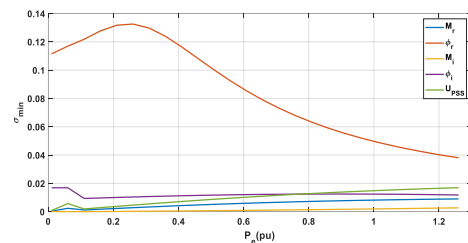


Fig.10. SVD Results

The results of the RGA and SVD criteria show that the best input for the supplementary control signal of the damper in a power system equipped with VSC HVDC is the rectifier phase angle. Therefore, this input will be used to design the controller proposed in this paper.

The results of plotting the damping function for the oscillatory mode at different operating points of the system are shown in Figure 11. It can be seen that the damping is at its lowest value for any of the system inputs under light operating conditions. The controller must be configured to provide sufficient damping for the network. This controller must ensure the necessary damping for oscillations under operating conditions of  $P_e = 0.65$ , which represents the worst conditions in terms of oscillatory mode damping. Therefore, the proposed controller is designed based on this operating point.

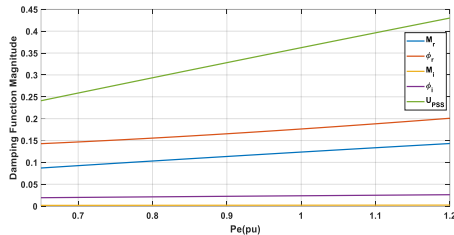


Fig.11. DF Results - Damping of oscillation mode over the operating condition

Table 1.  
Classic Controller Design

	$M_r$	$\varphi_r$	$\varphi_i$
$T_1$	0.28	0.39	5.2
$T_2$	0.31	0.42	0.03
$K_{dc}$	-53	-79.1	11.1

Based on the above results, a supplementary controller is used in the path between rotor speed changes and the rectifier modulation phase angle in VSC HVDC. The operating point of the power system for the design of this controller is  $P_e = 0.65$ . Using the phase compensation method, the classical controller is designed in various directions. The coefficients of this controller are provided in Table 1.

Figures 12, 13, and 14 show the results of the simulation of the linearized system in the presence of the proposed classical damper controllers (based on the coefficients in Table 1). The mechanical power deviation is considered 0.05pu as input disturbance to the synchronous generator. It can be seen that the best damping of power fluctuations (Figure 12), frequency fluctuations (Figure 13), and load angle (Figure 14) is achieved by the controller designed for the rectifier phase angle. Although other controllers provide the necessary damping for the stable operation of the power system, the settling time and overshoot of the output signals are minimized using the controller in the direction of the rectifier phase angle.

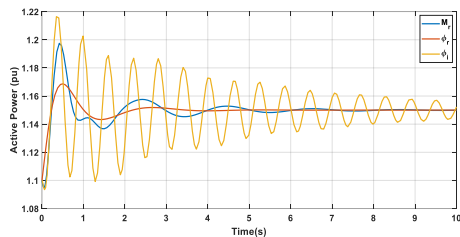


Fig.12. Generated Active Power in Synchronous Generator

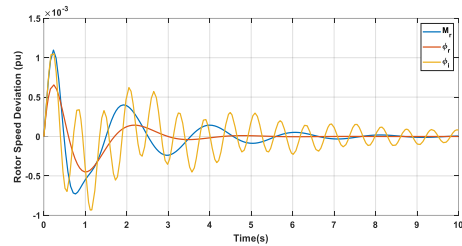


Fig.13. Rotor Speed Deviation in Synchronous Generator

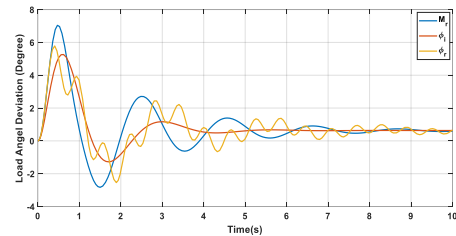


Fig.14. Load Angel Deviation in Synchronous Generator

The neural network adaptive controller is designed to dampen power system fluctuations. This controller is implemented using S-function functions in MATLAB software. For comparison purposes, the performance of the adaptive neural controller (ANN) and the classical controller in damping oscillations by applying a damping signal to the rectifier phase angle is evaluated first. The heavy system working condition ( $P_e=1.1pu$ ) is considered. The simulation results are presented in Figures 15, 16, and 17. It is evident that the adaptive neural controller outperforms the classical controller in damping frequency-power fluctuations significantly. Specifically, the settling time and overshoot of the output signals have been significantly reduced by the adaptive neural controller. Some neural controller weights are shown in Figure 17.

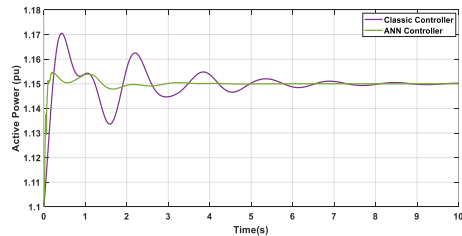


Fig.15. Generated Active Power in Synchronous Generator

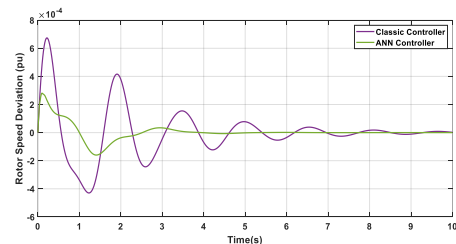


Fig.16. Rotor Speed Deviation in Synchronous Generator

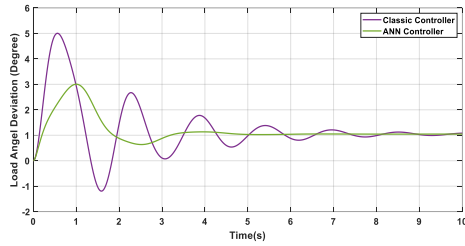


Fig.17. Load Angle Deviation in Synchronous Generator

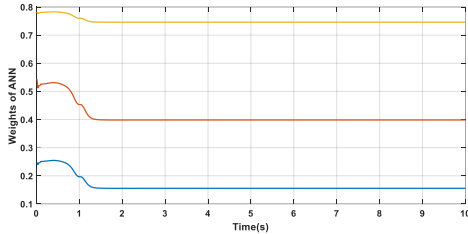


Fig.18. ANN Weights

Both classical and neural controllers are utilized to dampen the oscillations caused by load change disturbances in the turbine (at  $t=0s$  and  $P_m=0.05pu$ ), as well as three-phase short circuits (for 6 cycles at time  $t=5s$ ). The results of the simulation for these conditions are depicted in figures (19) and (20). It is evident that both controllers effectively mitigate the fluctuations in frequency and power. However, the adaptive neural controller outperforms the classical controller in terms of overshoot and settling time.

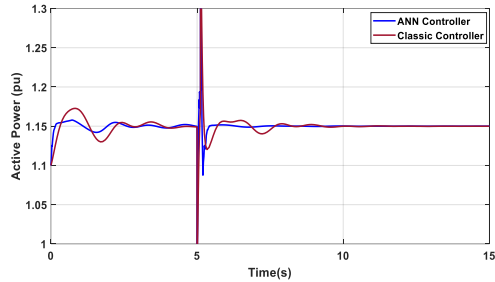


Fig.19. Generated Active Power in Synchronous Generator (Nonlinear System)

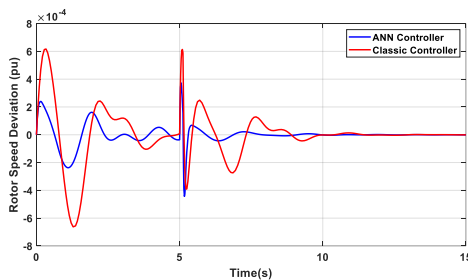


Fig.20. Rotor Speed Deviation in Synchronous Generator (Nonlinear System)

## 5. Conclusion

The study introduces a novel approach for modelling parallel AC/DC power systems and evaluates the effectiveness of classical and neural controllers in mitigating power system fluctuations. Simulation results, conducted using MATLAB, demonstrate the superior performance of the adaptive neural controller compared to the classical controller, particularly in terms of overshoot and settling time, under heavy system working conditions. These findings contribute to the advancement of control strategies for voltage source converter (VSC) HVDC systems, offering potential applications in enhancing transient stability and power oscillation damping.

## Appendix

Adaptive Neural Controller (for Both Neural Identifier and Controller): 3 layer feedforward Neural Network (Input Layer: 3 Neurons, Hidden Layer: 6 Neurons, Output Layer: 1 Neuron), Activation Function: Sigmoid, Sampling Time:  $1E-6$ ; Learning Rate: 0.1.

$P_e=1.1$ ;  $Q_e=0.3$ ;  $X_q=.6$ ;  $X_d=1$ ;  $X_{dp}=.3$ ;  
 $X_{tl}=.18$ ;  $X_{lb}=1$ ;  $X_s=.18$ ;  $X_{sp}=.18$ ;  
 $V_{dcr}=2$ ;  $V_{dci}=2$ ;  $C_{dcr}=1$ ;  $C_{dci}=1$ ;  $P_{ac}=P_e*(.5)$ ;  
 $P_{dc}=P_e-P_{ac}$ ;  $L_n=0.06$ ;  $T_{dop}=4$ ;  $M=12$ ;  $D=0$ ;  $K_a=45$ ;  
 $T_a=0.03$ ;  $K_a=140$ ;  $T_a=.015$ ;  $B=X_l/X_r$ ;  
 $Z=1+(X_l/X_r)$ ;  $A=X_t+X_l+(X_t*X_l)/X_r$ ;  
 $AA=A+(Z*X_{dp})$ ;  $BB=A+(Z*X_q)$ ;  $V_{dc}=V_{dcr}$ ;  
 $C_1=V_{bq}/BB$ ;  $C_2=-((X_l)/(2*BB*X_r))*$   
 $Mr*V_{dc}*\sin(PHr)$ ;  $C_3=((X_l)/(2*BB*X_r))*$   
 $V_{dc}*\cos(PHr)$ ;  
 $C_4=(X_l/(2*BB*X_r))* Mr*\cos(PHr)$ ;  $C_5=Z/AA$ ;  
 $C_6=(V_{bd})/AA$ ;  $C_7=-((X_l)/(2*AA*X_r))*$   
 $Mr*V_{dc}*\cos(PHr)$ ;  $C_8=-((X_l)/(2*AA*X_r))*$   
 $V_{dc}*\sin(PHr)$ ;  $C_9=-((X_l)/(2*AA*X_r))*$   
 $Mr*\sin(PHr)$ ;  $C_{11}=E_{qp}+((X_q-X_{dp})*I_{td})$ ;  
 $C_{12}=(X_q-X_{dp})*I_{tq}$ ;  $K_1=((C_{11}*C_1)+$   
 $(C_{12}*C_6))$ ;  $K_2=((I_{tq})*(1+(X_q-X_{dp})*C_5))$ ;  
 $K_{pdcr}=((C_{11}*C_4) + (C_{12}*C_9))$ ;  
 $K_{pnr}=((C_{11}*C_3) + (C_{12}*C_8))$ ;  
 $K_{pphr}=((C_{11}*C_2)+(C_{12}*C_7))$ ;  $J=X_d-X_{dp}$ ;  
 $K_3=1+(J*C_5)$ ;  $K_4=J*C_6$ ;  $K_{qphr}=J*C_7$ ;  $K_{qnr}=J*C_8$ ;  
 $K_{qdcr}=J*C_9$ ;  $L=(1/V_t)$ ;  $K_5=L*((V_{td}*X_q*C_1)-$   
 $(V_{tq}*X_{dp}*C_6))$ ;  $K_6=L*(V_{tq}*(1-(X_{dp}*C_5))$ ;  
 $K_{vdcr}=L*(V_{td}*X_q*C_4 - V_{tq}*X_{dp}*C_9)$ ;  
 $K_{vmr}=L*(V_{td}*X_q*C_3 - V_{tq}*X_{dp}*C_8)$ ;  
 $K_{vphr}=L*(V_{td}*X_q*C_2 - V_{tq}*X_{dp}*C_7)$ ;  
 $E=(X_t+X_{dp})/X_r$ ;  $C_{10}=E*C_5-(1/X_r)$ ;  $C_{11}=E*C_6$ ;  
 $C_{12}=E*C_7-((Mr*V_{dcr}*\sin(PHr))/(2*X_r))$ ;  
 $C_{13}=E*C_8+((V_{dcr}*\sin(PHr))/(2*X_r))$ ;  
 $C_{14}=E*C_9+((Mr*\cos(PHr))/(2*X_r))$ ;  
 $F=(X_q+X_t)/X_r$ ;  $C_{15}=F*C_1$ ;  
 $C_{16}=F*C_2+((Mr*V_{dcr}*\sin(PHr))/(2*X_r))$ ;  
 $C_{17}=F*C_4-((Mr*\cos(PHr))/(2*X_r))$ ;  
 $C_{18}=F*C_3-((V_{dcr}*\cos(PHr))/(2*X_r))$ ;  
 $C_{19}=V_{bd}/X_i$ ;  $C_{20}=M_i*\sin(PH_i)/(2*X_i)$ ;  
 $C_{21}=V_{dci}*\sin(PH_i)/(2*X_i)$ ;  
 $C_{22}=M_i*V_{dci}*\cos(PH_i)/(2*X_i)$ ;  
 $C_{23}=V_{bq}/X_i$ ;  $C_{24}=-((M_i*\cos(PH_i))/(2*X_i))$ ;  
 $C_{25}=-((V_{dci}*\cos(PH_i))/(2*X_i))$ ;  
 $C_{26}=(M_i*V_{dci}*\sin(PH_i))/(2*X_i)$ ;  
 $f_5=-0.5*(\cos(PHr)*I_{rd} + \sin(PHr)*I_{rq})$

$$f6=-0.5*(Mr*\sin(PHr)*Ird+Mr*\cos(PHr)*Ird);$$

$$f7=-0.5*Mr*\cos(PHr); f8=-0.5*Mr*\sin(PHr);$$

$$C31=f7*C11+f8*C15; C32=f7*C10;$$

$$C33=f7*C14+f8*C17; C34=f5+f7*C13+f8*C18;$$

$$C35=f6+f7*C12+f8*C16; f1=-0.5*(\cos(\Phi)*Iid + \sin(\Phi)*Iiq);$$

$$f2=-0.5*(-Mi*Iid*\sin(\Phi) + Mi*Iiq*\cos(\Phi)); f3=-0.5*Mi*\cos(\Phi); f4=-0.5*Mi*\sin(\Phi);$$

$$C27=f3*C19+f4*C23; C28=f3*C20+f4*C24; C29=f1+f3*C21+f4*C25;$$

$$C30=f2+f3*C22+f4*C26; Wb=2*\pi*Frequency;$$

$$P1=2*Xq*Itd; P2=2*Xdp*Itd; P3=P2-Eqp; P4=-Itd;$$

$$q1=P1*C1+P3*C6; q2=P3*C5+P4;$$

$$q3=P1*C4+P3*C9; q4=P1*C2+P3*C7;$$

$$q5=P1*C3+P3*C8;$$

## References

- [1] Abedin, T., Lipu, M. S. H., Hannan, M. A., Ker, P. J., Rahman, S. A., Yaw, C. T., & Muttaqi, K. M. (2021). Dynamic modeling of hvdc for power system stability assessment: A review, issues, and recommendations. *Energies*, 14(16), 4829.
- [2] Watson, N. R., & Watson, J. D. (2020). An overview of HVDC technology. *Energies*, 13(17), 4342.
- [3] Amrr, S. M., Asghar, M. J., Ashraf, I., & Meraj, M. (2020). A comprehensive review of power flow controllers in interconnected power system networks. *IEEE Access*, 8, 18036-18063.
- [4] Machowski, J., Lubosny, Z., Bialek, J. W., & Bumby, J. R. (2020). *Power system dynamics: stability and control*. John Wiley & Sons.
- [5] Wang, L., Ertugrul, N., & Negnevitsky, M. (2022). Enhancement of the System Stability of DB-Controlled VSC Links Parallel Operated with a Weak Multi-Machine AC Power System. *Energies*, 15(7), 2424.
- [6] Hatziaargyriou, N., Milanović, J., Rahmann, C., Ajarapu, V., Cañizares, C., Erlich, I., ... & Vournas, C. (2020). Stability definitions and characterization of dynamic behavior in systems with high penetration of power electronic interfaced technologies. *IEEE PES Technical Report PES-TR77*.
- [7] Khampariya, P., Panda, S., Alharbi, H., Abdelaziz, A. Y., & Ghoneim, S. S. (2022). Coordinated Design of Type-2 Fuzzy Lead-Lag-Structured SSSCs and PSSs for Power System Stability Improvement. *Sustainability*, 14(11), 6656.
- [8] Meng, Y., Wang, H., Duan, Z., Jia, F., Du, Z., & Wang, X. (2022). Small-Signal Stability Analysis and Improvement with Phase-Shift Phase-Locked Loop Based on Back Electromotive Force Observer for VSC-HVDC in Weak Grids. *Journal of Modern Power Systems and Clean Energy*.
- [9] Zhu, J., Wang, X., Zhao, J., Yu, L., Li, S., Li, Y., ... & Wang, C. (2022). Inertia Emulation and Fast Frequency-Droop Control Strategy of a Point-to-Point VSC-HVdc Transmission System for Asynchronous Grid Interconnection. *IEEE Transactions on Power Electronics*, 37(6), 6530-6543.
- [10] Ramadhan, U. F., Suh, J., Hwang, S., Lee, J., & Yoon, M. (2022). A Comprehensive Study of HVDC Link with Reserve Operation Control in a Multi-Infed Direct Current Power System. *Sustainability*, 14(10), 6091.
- [11] Banaei, M. R., & Taheri, N. (2011). An adaptive neural damping controller for HVDC transmission systems. *European Transactions on Electrical Power*, 21(1), 910-923.
- [12] Taheri, N., Orojlo, H., & Ebrahimi, F. (2022). Damping controller design in offshore wind power plants to improve power system stability using fractional order PID controllers based on optimized exchange market algorithm. *Journal of Intelligent Procedures in Electrical Technology*, 13(51), 91-110.
- [13] Taheri, N., Orojlo, H., Karimi, H., Ebrahimi, F., & Khalifeh, K. (2021). Novel Adaptive Damping Controller for Interline Power Flow Controller to Improve Power System Stability. *International Journal of Smart Electrical Engineering*, 10(04), 225-234.
- [14] Hamidi, A., Beiza, J., Abedinzadeh, T., & Daghigh, A. (2022). Robust Power Designing of Supplementary Damping Controller in VSC HVDC System to Improve Energy Conversion Efficiency of Wind Turbine and Power System Stability. *Journal of Electrical and Computer Engineering*, 2022.
- [15] Zhou, T., Chen, Z., Ren, B., Bu, S., & Wang, P. (2020). Damping Torque Analysis of VSC-HVDC Supplementary Damping Controller for Small-Signal Stability. *IEEE Access*, 8, 202696-202706.
- [16] Gupta, P., Pal, A., & Vittal, V. (2020). Coordinated wide-area control of multiple controllers in a power system embedded with HVDC lines. *IEEE Transactions on Power Systems*, 36(1), 648-658.
- [17] Klamka, J. (2013). Controllability of dynamical systems. A survey. *Bulletin of the Polish Academy of Sciences: Technical Sciences*, (2).
- [18] Allahyari, S. A., Taheri, N., Zadehbagheri, M., & Rahimkhani, Z. (2018). A novel adaptive neural MPPT algorithm for photovoltaic system. *International Journal of Automotive and Mechanical Engineering*, 15(3), 5421-5434.
- [19] Shafaghatian, N., Kiani, A., Taheri, N., Rahimkhani, Z., & Masoumi, S. S. (2020). Damping controller design based on FO-PID-EMA in VSC HVDC system to improve stability of hybrid power system. *Journal of Central South University*, 27(2), 403-417.
- [20] Taheri N. Novel Adaptive Recurrent Neural Controller based on VSC HVDC Damping Controller to Improve Power System Stability. *International Journal of Smart Electrical Engineering*. 2023 Feb 1;12(01):51-9.